



Contents lists available at ScienceDirect

Applied Clay Science

journal homepage: www.elsevier.com/locate/clay

Research paper

Experimental and modeling investigations of cesium and strontium adsorption onto clay of radioactive waste disposal

Abdel-Aal M. Abdel-Karim^{a,*}, Ahmed A. Zaki^b, Waheed Elwan^a,
Mohamed R. El-Naggar^b, Mahmoud M. Gouda^b

^a Geology Department, Faculty of Science, Zagazig University, Zagazig, Egypt

^b Hot Lab. Center, Atomic Energy Authority, P.O. 13759, Cairo, Egypt

ARTICLE INFO

Article history:

Received 17 March 2016

Received in revised form 15 June 2016

Accepted 10 July 2016

Available online xxx

Keywords:

Clay

Weathering

Cesium

Strontium

Sorption

Kinetics and thermodynamics

ABSTRACT

Migration of strontium and cesium radionuclide in geohydraulic system is important for safety disposal of radioactive waste containing of these two radionuclides to prevent the migration of radionuclides from the disposal site to provide protection for man and his environment. Geochemical analysis was carried out to investigate the mineral composition of the clay taken from the site to predict the historical and environmental geology of Inshas disposal site. Batch experiments were carried out as a function of pH, solute concentration and under three different temperatures (298°, 313° and 333° K). Sorption capacity of Cs⁺ and Sr²⁺ onto clay sample was increased when initial metal ions concentration was increased. Increasing the temperature led to decrease in the sorption of Cs⁺ and Sr²⁺ ions. Several kinetic models were used to fit the experimental data and to examine the controlling mechanisms of the sorption processes. The kinetic study showed that sorption followed pseudo-second-order model with a good correlation coefficient ($R^2 = 0.999$) for both studied ions. The experimental sorption data were fitted using Freundlich, Langmuir and Dubinin–Radushkevich (D–R) models. Results showed that the adsorption process was exothermic and favored at low temperature.

© 2016 Elsevier B.V. All rights reserved.

1. Introduction

The generated radioactive waste can be divided into liquid, solid and gaseous wastes. Aqueous liquid radioactive waste was generated during research reactor operations and in other operations involving the application of radioisotopes (e.g. medicine, research and education). The type of liquid waste produced depends upon the particular operation being conducted and can vary extensively in both chemical and radionuclides content. In a radioactive waste repository, the main protective function provided by natural geological barrier itself, selected in such a way that its impermeability and stability characteristics should prevent contamination to reach to biosphere.

On the other hand, due to the negative evolution of the radioactive waste repository over hundreds or thousands of years, the natural or engineered barriers are deteriorated. As a result many scenarios, which could lead to leak of the radioactive such as intrusion of rain or ground water, leaching of waste containers, etc. are suggested (Alves et al., 2015; Abdel Rahman et al., 2009; Abdel Rahman et al., 2007; Abdel Rahman and Zaki, 2011).

In this regard, a primary concern is the contamination of groundwater that is considered a very important vector of pollution. Any accidental release of aqueous waste solutions containing both cesium and strontium may pose an environmental health risk to the soil/groundwater system (Tianlik et al., 2016). The fate and transport of individual contaminants into an aqueous phase is largely controlled by the degree of contaminant interaction with the surrounding soil materials. Distribution coefficient (K_d) is a parameter was used to present the ratio of ions adsorbed into solid to ions in liquid phase (Kamel and Navratil, 2002) this parameter can be influenced by concentration of the stable elements in soil/aqueous phase.

Clay minerals are important group of minerals because they are among the most common products of chemical weathering of rocks. Clay minerals are important sorbents for radionuclides due to their negative charge, large specific surface area and surface hydroxyl groups. Sorption on clay minerals strongly affects the fate and mobility of radioactive contaminants in the geosphere (Seung and Diwakar, 2012; Zaki et al., 2011). Different clay minerals show different sorption capacities for radionuclides (Deepthi Rani and Sasidhar, 2011). Their high specific surface area allows strong physical and chemical interactions with fluids and dissolved species which are subjected to electrostatic repulsion, sorption or specific cation exchange reactions. These interactions are responsive for the retention in the barrier of leachate components

* Corresponding author.

E-mail addresses: Am_abdelkarim@hotmail.com, amabdelkarim@zu.edu.eg (A.-A.M. Abdel-Karim).

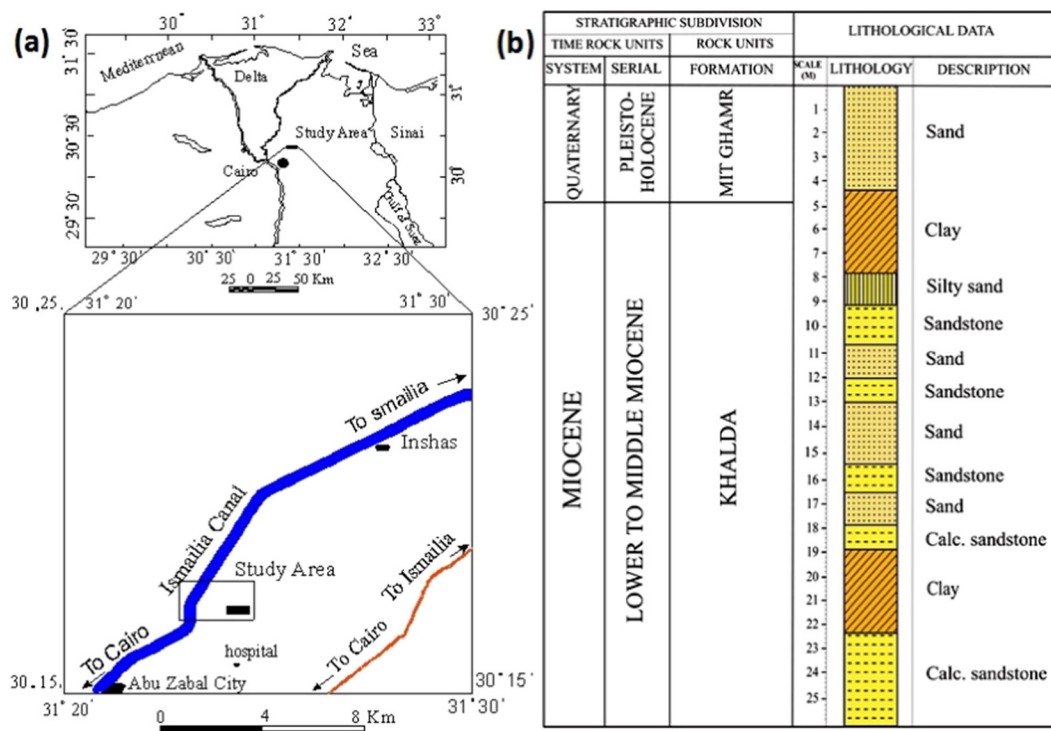


Fig. 1. a. Location map and b. Litho-stratigraphic units of borehole B2 of the study area.

such as dangerous metallic cations (Churchman et al., 2006; Sánchez-Jiménez et al., 2012).

Inshas area (Fig. 1a) which is bounded by longitudes $31^{\circ} 20'$ & $31^{\circ} 40'$ E and latitudes $30^{\circ} 10'$ & $30^{\circ} 25'$ N is considered as an important region for the Egyptian Atomic Energy Authority (EAEA). An area of approximately $1 \text{ km} \times 1 \text{ km}$ dimensions had been chosen to be exposed to detailed geologic studies. The main purposes of such studies are standing on the lithological succession in the subsurface. The litho-stratigraphy of studied borehole B2 shows a succession of quaternary and tertiary sediments which are arranged from bottom to top (Fig. 1b) into: a) quaternary sediments which is represented by sands, and b) tertiary sediments which are composed of Miocene clays, silty sand, sand, sandstone and calcareous sandstone (Zaki, 2000).

The aim of this work is to study the geochemical and chemical feasibility of the clay as a sorptive barrier towards cesium and strontium ions of Inshas radioactive disposal site.

2. Materials and methods

2.1. Chemicals and reagents

The chemicals and reagents used for cesium and strontium ions were supplied as cesium chloride and strontium chloride, and obtained from Sigma-Aldrich Company. All solutions were prepared using distilled, deionized water (DDW) with a resistivity of $18 \text{ M}\Omega/\text{cm}$. Stock solutions of the test reagents were prepared by dissolving CsCl and $\text{SrCl}_2 \cdot 6\text{H}_2\text{O}$ in DDW. Clay soil samples were obtained from Inshas disposal site (Fig. 1a).

2.2. Characterization of clay

The clay samples were dried, crushed and sieved through the $38\text{-}\mu\text{m}$ sieve. Clay samples were characterized using X-ray diffractometer; Philips X-ray diffraction equipment model PW 1710 with monochromator, Cu-radiation ($\lambda = 1.542 \text{ \AA}$). In order to separate the clay particles

($<2 \mu\text{m}$) from the bulk soil sample, the bulk sample was put in a DDW beaker for 7 h, then the supernate was poured in another beaker with 3 glass slides on the bottom and kept for about 24 h. To identify the exact clay minerals in the sample, the above mentioned slides were separately treated. The first slide was kept without any treatment (air dried), whereas the second was heated to 823 K for 2 h and the third was exposed to glycerol vapor in a desiccator for 2 h, then the subsamples were measured by the diffractometer.

Scanning electron microscopy (Philips, XL 30), Fourier transform infrared spectroscopy (BOMEM FTIR, MB-Series) were used to test the function groups and surface formology of the clay sample, respectively. The average particles of the clay samples were ranged from 10 to $35 \mu\text{m}$ on the basis of SEM results. Moreover, this average attain about $0.001\text{--}0.003 \text{ mm}$ by using high-magnified polarizing microscope method for comparison. The elemental composition of the clay was measured using an XRF-1800 SHIMADZU sequential XRF spectrometer with a rhodium tube and a 2.5 kW generator. The detection limit was about $0.01 \text{ wt.}\%$ and analytical precision (relative standard deviation) was $<1\%$ for major elements.

2.3. Batch sorption/desorption studies

A series of batch sorption tests were conducted using clay at pH ranged from 2 to 12. The pH of solutions was adjusted using (0.1 M) of NaOH and HCl. A weighed amount (0.1 g) of the sorbent was introduced into reagent bottles (each containing 10 ml of cesium or strontium ions at 100, 500 or 1000 mg/l concentration). Bottles were shaken at 298°K using a mechanical shaker for 24 h to attain equilibrium. After separating the supernatant liquid by centrifugation at 6000 rpm for 30 min cesium and strontium ions concentration in the supernatant was determined using atomic absorption spectrophotometer (AAS; Buck Scientific, VGP-210). The desorption experiments were conducted at 298°K , where 0.1 g of the loaded clay with Cs^+ or Sr^{2+} were shaken with 10 ml of 0.5 M HCl and centrifuged at 6000 rpm for 30 min and checked at different times using AAS. In all adsorption and

desorption experiments, the runs were repeated three times for a given data point and the average was considered. The effect of pH was evaluated by calculating the sorption uptake by Eq. (1):

$$\text{Sorption uptake (\%)} = \frac{C_0 - C_e}{C_0} \times 100 \quad (1)$$

where C_0 and C_e are the initial and final concentrations (mg/l).

2.3.1. Kinetic experiments

Kinetic studies were investigated at a constant initial Cs^+ and Sr^{2+} concentration of (100 mg/l) and three different temperatures (298°, 313° and 333° K) where 0.1 g of the clay was contacted with 10 ml of aqueous solution. The withdrawn solution was centrifuged at 6000 rpm for 30 min. to separate the sorbent and a fixed volume of the clear solution was pipetted out for the determination of the amount of unadsorbed metal ion. The amount of Cs^+ and Sr^{2+} sorbed onto clay (mg/g) can be calculated by Eq. (2),

$$q_e = \frac{(C_0 - C_e) \times V}{m} \quad (2)$$

where V is the volume of the solution in liters and m is the mass of the clay in grams.

2.3.2. Sorption isotherm modeling

Langmuir, Freundlich and Dubinin–Radushkevich (D–R) models were used to calculate the theoretical sorption capacity. Experiments were performed using 10 ml of the metal ion solution of varying concentrations (50–1000 mg/l) at pH = 7.0 with 0.1 g of clay at different temperatures (298, 313 and 333° K) and were kept overnight to reach equilibrium.

3. Results and discussion

3.1. Characterization of the clay

To get the mineral composition of Inshas clay soils from the disposal site, three samples of clay were taken and were measured by X-ray fluorescence (XRF) spectroscopy. Different Si/Al ratios were observed and given in Table 1. The sample number 1 was selected because it has the largest amount of Al_2O_3 , which can play a role in ion exchange process of the studied metal ions. Fig. 2a shows the X-ray diffraction pattern of the analyzed clay, which isolated from the bulk clay sample soil of Inshas disposal site. In this figure, the clay minerals of the sample are represented by kaolinite, vermiculite, illite, calcite and plagioclase feldspar. Based on the basal d-spacing (Å), the single minerals as illite was obtained at 10, 3.33, 4.46 Å, vermiculite was observed at 14 Å which was changed by heating to be observed at 10 Å, kaolinite was observed at 7 Å but is destroyed by heating, calcite was obtained at 3.03 Å and plagioclase feldspar at 3.2 Å. Also, the diffraction pattern shows that the illite, plagioclase feldspar, and calcite are exist before and after treatment at the same 2θ . Illite exists at 9°, 20° and 27° in 2θ . Plagioclase feldspar exists at 28° in 2θ , while calcite appears at 29.5° in 2θ . On the other hand, the peak represents vermiculite shifted from 6° to 8.5° in 2θ , due to exposing to glycerol vapor. Moreover, kaolinite was destroyed due to heating of clay to 823° K for 2 h; kaolinite peaks at 12.5° and 25° in 2θ for air dried and that exposed to glycerol vapor disappeared in the heat treated sample (Harley et al., 2015).

Table 1
Quantitative elemental analysis (%) of the clay samples from Inshas disposal site.

Sample	Na ₂ O	MgO	Al ₂ O ₃	SiO ₂	K ₂ O	CaO	TiO ₂	Cr ₂ O ₃	MnO	Fe ₂ O ₃	Cl	LOI	Total
i	1.78	2.61	17.74	52.42	1.51	7.24	2.88	0.02	0.06	9.85	0.91	2.98	100
ii	1.30	2.95	16.63	53.69	1.53	7.04	2.71	0.05	0.23	10.07	0.86	2.94	100
iii	1.58	3.09	15.45	51.08	1.66	7.97	2.20	0.05	0.21	11.73	1.34	3.64	100

3.2. FTIR spectral analysis

The FTIR spectra of the used bulk clay sample in the range of 500–4000 cm^{-1} was taken to confirm the presence of functional groups that are usually responsible for the sorption process (Fig. 2b). There are a number of absorption peaks, reflecting the complex nature of the clay. The spectrum shows the presence of bands arising at 3695, and 3624 cm^{-1} are characteristic of kaolinite OH vibration bands. At 1031, 3930, 915, 535 and 476 cm^{-1} retraces the characteristic bands of kaolinite (Martinez et al., 2010) and halloysite. The bands 467 and 535 cm^{-1} are attributed to Si–O–Si, and Al–O–Si bending vibration, respectively (Van der Marel and Beutelspacher, 1976; Runliang et al., 2008). Absorption at 1637 cm^{-1} retraces the characteristic bands of calcite. The band of absorbance in the range between 3700 and 3000 cm^{-1} of the studied sample results from H₂O stretching vibrations.

TGA-DTA curves of the clay sample are presented in Fig. 2c. In this figure, the first small endothermic peak occurs at 423° K is related to loss of adsorbed water causing mass weight loss (about 2.33%), which may be due to removal of external water molecule. There are endothermic peaks at 848.67° K and 973.66° K with weight loss of 2.33% and 5.90, respectively, which could be attributed to the dehydration of kaolinite (Paola et al., 2015). It is also remarked that a disappearance of the kaolinite peaks in the X-ray pattern of the thermally treated clay sample. The total mass weight loss of about 6.12% is up to 1273° K.

Scanning electron microscopy (SEM) image describes the shape of the structure of minerals in the studied clay sample, which found as irregular shaped grains as shown in Fig. 2d.

3.3. Geochemistry of clay

The results of major elements analysis of three samples of clay from Inshas disposal site, Cairo, Egypt are presented in Table 1. The chemical composition of the samples indicates that SiO₂, Al₂O₃, Fe₂O₃ and CaO are the major constituents besides minor Na₂O, MgO, TiO₂, K₂O, MnO. The obtained data can be utilized to deduce the provenance of the source rock, the degree of chemical weathering, and maturity and climatic conditions during sedimentation that explain as follows:

3.3.1. Provenance

The Major element provenance discriminant function diagram for the samples sands (Shaohao et al., 2016), as given by Eqs. (3) and (4):

$$\begin{aligned} \text{Discriminant function 1} = & (-1.773 \times \text{TiO}_2) + (0.607 \times \text{Al}_2\text{O}_3) \\ & + (0.760 \times \text{Fe}_2\text{O}_3) + (-0.50 \times \text{MgO}) + (0.616 \times \text{CaO}) + (0.509 \\ & \times \text{Na}_2\text{O}) + (-1.224 \times \text{K}_2\text{O}) + (9.09). \end{aligned} \quad (3)$$

$$\begin{aligned} \text{Discriminant function 2} = & (0.445 \times \text{TiO}_2) + (0.07 \times \text{Al}_2\text{O}_3) \\ & + (-0.25 \times \text{Fe}_2\text{O}_3) + (-1.142 \times \text{MgO}) + (0.438 \times \text{CaO}) \\ & + (1.475 \times \text{Na}_2\text{O}) + (1.426 \times \text{K}_2\text{O}) + (-6.861). \end{aligned} \quad (4)$$

The diagram discriminates (4) major provenance categories of mafic (P₁), intermediate (P₂), felsic (P₃), and quartzose recycled (P₄) (Sahraeyan and Bahrami, 2012). This discriminant function diagram indicates a mafic igneous source for the studied samples as shown in Fig. 3a.

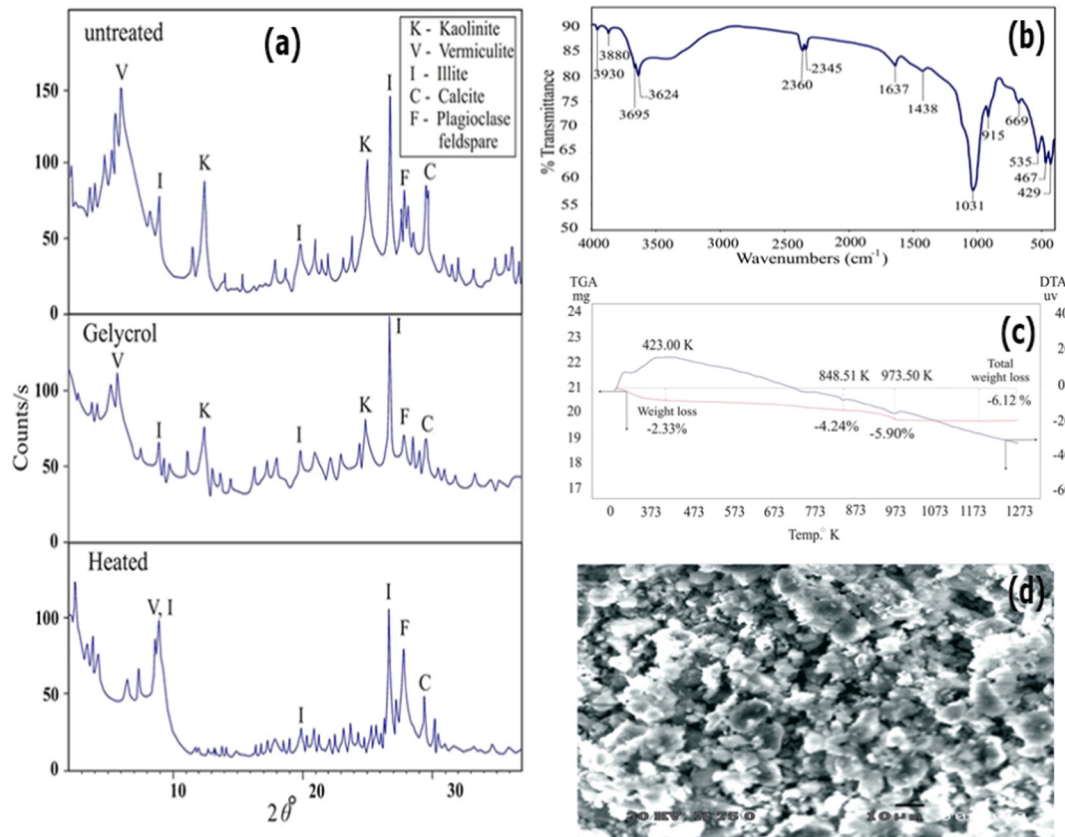


Fig. 2. Characterization of the studied clay showing: a. X-ray diffraction, b. FT-IR spectrum, c. TGA/DTA curves and d. Scanning electron microscopy image (SEM), X = 750.

3.3.2. Weathering in the source area

Geochemical parameters obtained from the analysis of sediments and sedimentary rocks are widely used to infer weathering and paleo-weathering conditions of source areas (Ohta and Arai, 2007; Eduardo and Alberto, 2016). Table 2 illustrated the calculation of the chemical index of alteration (Schneider et al., 2016), the chemical index of weathering (Sener, 2015), the plagioclase index of alteration (Frank et al., 2014), the mineralogical index of alteration (Voicu et al., 1997; Babechuk et al., 2014) were defined as in Eqs. (5)–(8).

$$\text{CIA} = 100 \times \text{Al}_2\text{O}_3 / (\text{Al}_2\text{O}_3 + \text{CaO} + \text{Na}_2\text{O} + \text{K}_2\text{O}) \quad (5)$$

$$\text{CIW} = (\text{Al}_2\text{O}_3 / (\text{Al}_2\text{O}_3 + \text{CaO} + \text{Na}_2\text{O})) \times 100 \quad (6)$$

$$\text{PIA} = [(\text{Al}_2\text{O}_3 - \text{K}_2\text{O}) / (\text{Al}_2\text{O}_3 + \text{CaO} + \text{Na}_2\text{O} - \text{K}_2\text{O})] \times 100 \quad (7)$$

$$\text{MIA} = 2 \times (\text{CIA} - 50) \quad (8)$$

In case of the values of the chemical index of alteration (CIA) are 100% means complete weathering of a primary material into its equivalent weathered product (Eduardo and Alberto, 2016; Voicu and Bardoux, 2002). The low CIA values of approximately 50 imply an un-weathered upper crust or weak weathering, but high CIA values (i.e. 76–100) indicate moderate weathering with a complete removal of alkali and alkaline earth elements and an increase in Al_2O_3 (Su et al., 2016; Etemad et al., 2011; Dupuis et al., 2006).

The average CIA values in samples in the range (68.64 to 73.73%), so the most samples have values > 60, suggesting moderate weathering either of the original source or during transport before deposition respectively while the average CIW values are in the range (74.61 to 79.55%) as in Table 2. The variation in CIA values reflected the changes in the proportion of clay minerals in the sandstone samples analyzed at the source area. The ranges of mineralogical index of alteration (MIA) values

indicate incipient (0–20%), weak (20–40%), moderate (40–60%), and intense to extreme (60–100%) weathering. The mineralogical index of alteration (MIA) have values average 41.73% indicating moderate weathering in samples (Hossain et al., 2014).

The plot of CIA versus Al_2O_3 depicts the most samples moderate degree of weathering of source materials as in shown in Fig. 3b. The degree of the chemical weathering estimated using the Plagioclase Index of Alteration (PIA) have values average of 74.42 indicating moderate weathering at the source.

3.3.3. Maturity and climatic conditions during sedimentation

Suttner and Dutta (1986) proposed a binary SiO_2 wt. percentage versus ($\text{Al}_2\text{O}_3 + \text{K}_2\text{O} + \text{Na}_2\text{O}$) wt. percentage diagram. Increasing in degree of chemical weathering may reflect the decreasing in tectonic activity and/or change in climate towards warm and humid conditions (Darcy et al., 2014; Sila et al., 2015). Chemical maturity of the samples indicating that the clay of the present study deposited under semiarid to arid conditions as shown in Fig. 3c.

3.4. Sorption batch investigations

The sorption of Cs^+ and Sr^{2+} from aqueous solution was tested experimentally to investigate the sorption capacities by studied clay sample (i) as behavior in case of releasing this radionuclide into geosphere in disposal site. The objective of this part of the study was to investigate equilibrium and kinetic parameters for the sorption of Cs^+ and Sr^{2+} ions onto the natural materials. The factors affecting on the sorption of the studied ions are tested by time of equilibration, the effect of V/m , hydrogen ion concentration, metal ion concentrations, temperature and by studying of some kinetic and isotherm models (Abdel Moamen et al., 2015).

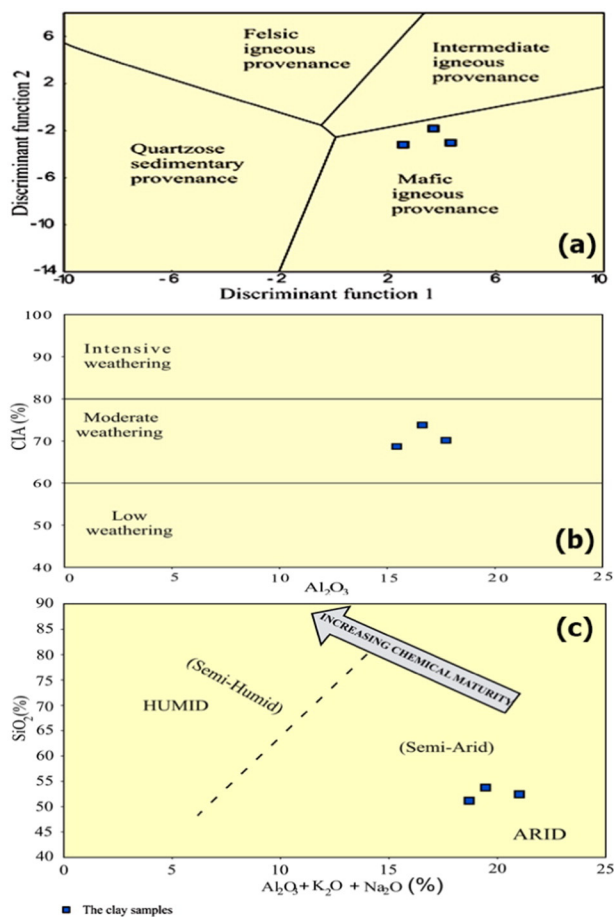


Fig. 3. Geochemistry of the analyzed clay showing: a. Provenience discriminant function diagram (after Roser and Korsch, 1988), b. Chemical index of alteration (CIA) versus Al_2O_3 and c. Chemical maturity expressed by SiO_2 versus $(\text{Al}_2\text{O}_3 + \text{K}_2\text{O} + \text{Na}_2\text{O})$ (after Suttner and Dutta, 1986).

3.4.1. Effect of contact time

The variation of amounts of Cs^+ and Sr^{2+} ions sorbed onto clay sample at $\text{pH} = 7.0$, different time intervals as well as different sorption temperatures (298° , 313° and 333° K) as shown in Fig. 4a. The experimental data showed that the amount of the metal ion sorbed increases gradually with time in the initial stage (20–30 min.), and then reach an equilibrium value at approximately 90 min. The sorption capacity of cesium ions by clay is higher due to the selectivity for cesium than for strontium (Po et al., 2010). The amounts of metal ion sorbed natural materials at any time, q_t (mg/g) is calculated from:

$$q_t = (C_0 - C_t) \left(\frac{V}{m} \right) \quad (9)$$

3.4.2. Effect of desorption

Fig. 4(b) shows desorption of both Cs^+ and Sr^{2+} from clay soil by 0.5 M HCl, at $\text{pH} 7.0$ and at room temperature. The percentage of

desorption was calculated using the following relation (Bucur et al., 2011):

$$D(\%) = \frac{m_{aq}^{des}}{m_s^{ads}} \cdot 100 \quad (10)$$

where: D (%) is desorption percentage, m_{aq}^{des} is the contaminant mass desorbed from the clay (mg/l), m_s^{ads} is the contaminant mass sorbed on sediment at sorption equilibrium (mg/l). It is clear from the figure that about 89.14 and 63.75% of Cs^+ and Sr^{2+} were desorbed, respectively at equilibrium after about 30 min for Cs^+ and 45 min for Sr^{2+} . Desorption experiments performed showed that Cs^+ and Sr^{2+} are partially reversibly sorbed on the clay soil from Inshas site. The high desorption of Cs^+ could be attributed to the high solubility of CsCl formed during the desorption process (Ziemer et al., 2006).

3.4.3. Effect of pH

The sorption was studied at different pH values in the range from 2.0 to 12.0 to determine the chemical condition at which Cs^+ and Sr^{2+} ions are effectively sorbed onto clay. It was observed that an increasing of amount sorbed of Cs^+ and Sr^{2+} by increasing of pH (Fig. 4b).

3.4.4. Effect of initial concentration

The amount sorbed (mg/g) of both Cs^+ and Sr^{2+} ions onto studied clay at three temperatures (298° , 313° and 333° K) by varying the initial metal ion concentration from 50 to 1000 mg/l are shown in Fig. 4c. All other parameters were constant. The Cs^+ and Sr^{2+} ions show that the sorption amount increased by increasing initial metal ion concentration and the amount of Cs^+ ions sorbed is higher than that of Sr^{2+} ions and the adsorption decreased by increasing in the temperature of an aqueous solution (Fig. 4c).

3.5. Kinetic modeling

Sorption kinetics was controlled by different mechanisms like mass transfer, diffusion control, and chemical reactions. Both pseudo first-order and pseudo second-order rate models include all steps of sorption in order to identify the controlling sorption mechanism. In order to clarify the kinetic characteristics of sorption of Cs^+ and Sr^{2+} ions onto the clay sample with the time, an appropriate kinetic model is required. For this purpose pseudo first-order and pseudo second-order rate models were studied.

3.5.1. Pseudo first-order kinetic model

The pseudo first-order kinetic model describes the sorption rate based on the sorption capacity. The model assumes that the reaction rate is limited by only one process or mechanism on a single class of sorbing sites and that all sites are of the time dependent type. The Lagergren pseudo first-order expression is given in Eq. (11)

$$\log(q_e - q_t) = \log q_e - \frac{k_1}{2.303} t \quad (11)$$

The plotting of $\log(q_e - q_t)$ versus time for Cs^+ and Sr^{2+} ions sorption onto clay is shown in Fig. 5a. Linear fitting of data was used to determine the first order rate constant (k_1) and the theoretical equilibrium sorption capacities (q_e), from the slopes and intercept respectively. Table 3 shows the results of kinetic studies of Cs^+ and Sr^{2+} sorbed onto studied clay. It seems that, although R^2 of each plot are so good, the q_e (calculated) values for Cs^+ and Sr^{2+} ions are not in agreement with q_e (experimental). Therefore, it could be suggested that the sorption of Cs^+ and Sr^{2+} ions is not a first-order reaction as concluded by McKay and Ho (1999).

Table 2

Weathering and alteration indices of the clay samples.

Index	Samples		
	i	ii	iii
CIA	70.24	73.73	68.64
PIA	73.25	77.80	72.20
CIW	75.10	79.55	74.61
MIA	40.48	47.46	37.29

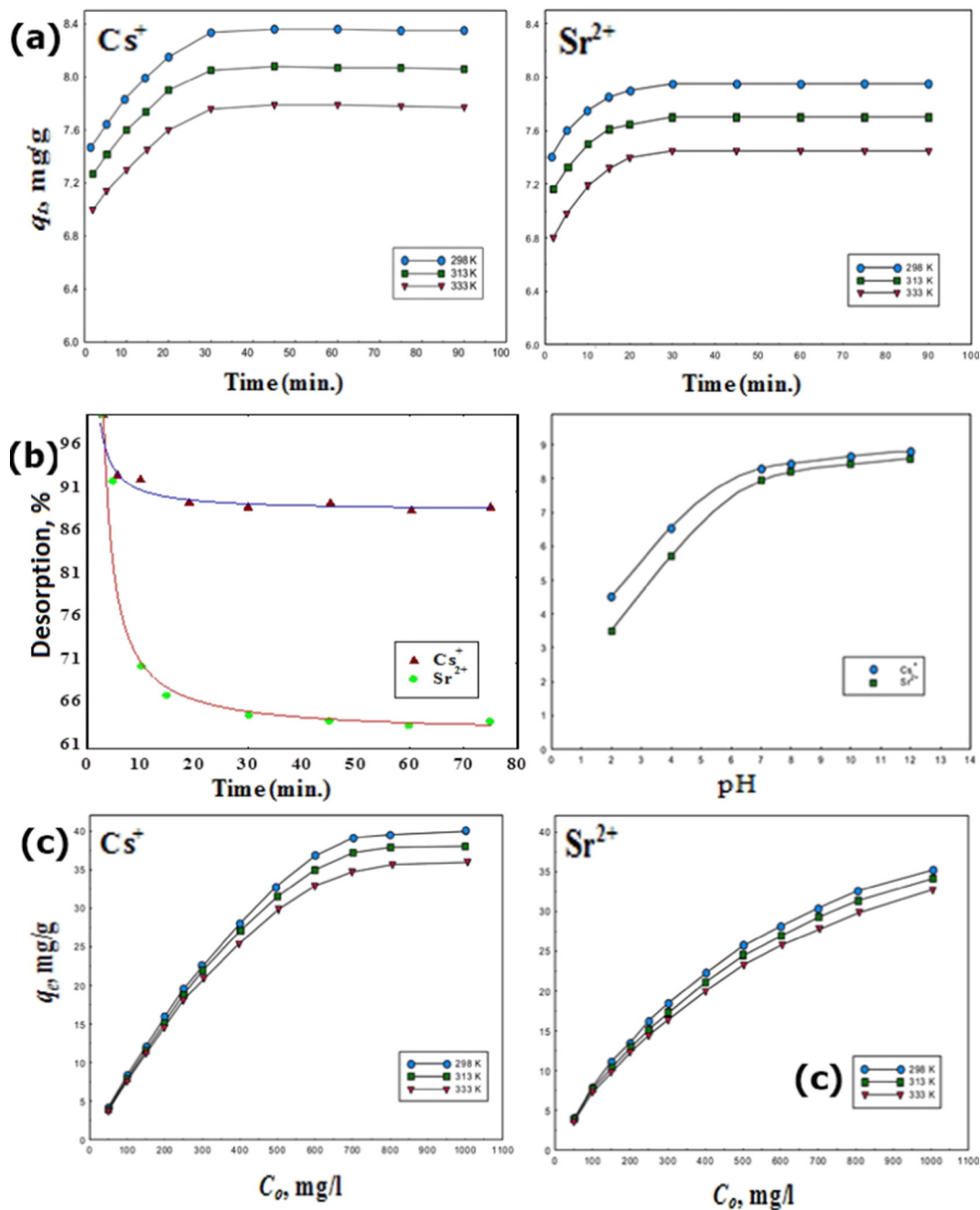


Fig. 4. Sorption batch investigations, kinetic modeling and desorption of Cs⁺ and Sr²⁺ onto studied clay sample at different temperatures showing: a. effect of contact time on sorption, b. effect of desorption versus time and pH on the sorption capacity, c. effect of initial concentration on amount of sorption.

3.5.2. Pseudo second-order kinetic model

A pseudo second-order rate model also used to describe the kinetics of the sorption of ions sorbed onto adsorbent materials. This model was expressed as:

$$\frac{t}{q_t} = \frac{1}{k_2 q_e^2} + \frac{1}{q_e} t \quad (12)$$

where k_2 is the rate constant of pseudo second-order equation (kg/mg min). The kinetic plots of t/q_t versus t for Cs⁺ and Sr²⁺ ions sorption observed in Fig. 5b.

The linear relationship and the values of the correlation coefficients (R^2) suggest strong relationships between their parameters and also explain that the process of sorption of ions follows the pseudo second-order kinetic model. The products $k_2 q_e^2$ is the initial sorption rate

which presented as $h = k_2 q_e^2$. The kinetic parameters of this model are calculated from the slopes and intercept of the linear plots (Table 3). The correlation coefficients are high and the theoretical and experimental q_e are closed to each other. Therefore, it is possible to suggest that the sorption of Cs⁺ and Sr²⁺ ions followed the pseudo-second order kinetic model for all studied sorption processes. These results explain that the pseudo second-order sorption mechanism is predominant and that the overall rate constant of each sorption process appears to be controlled by chemical sorption process (Talal, 2014).

3.6. Sorption isotherm models

Sorption equilibrium is usually described by an isotherm equation whose parameters express the surface properties and affinity of the sorbent at a fixed temperature and pH. Fig. 6a shows the relation between

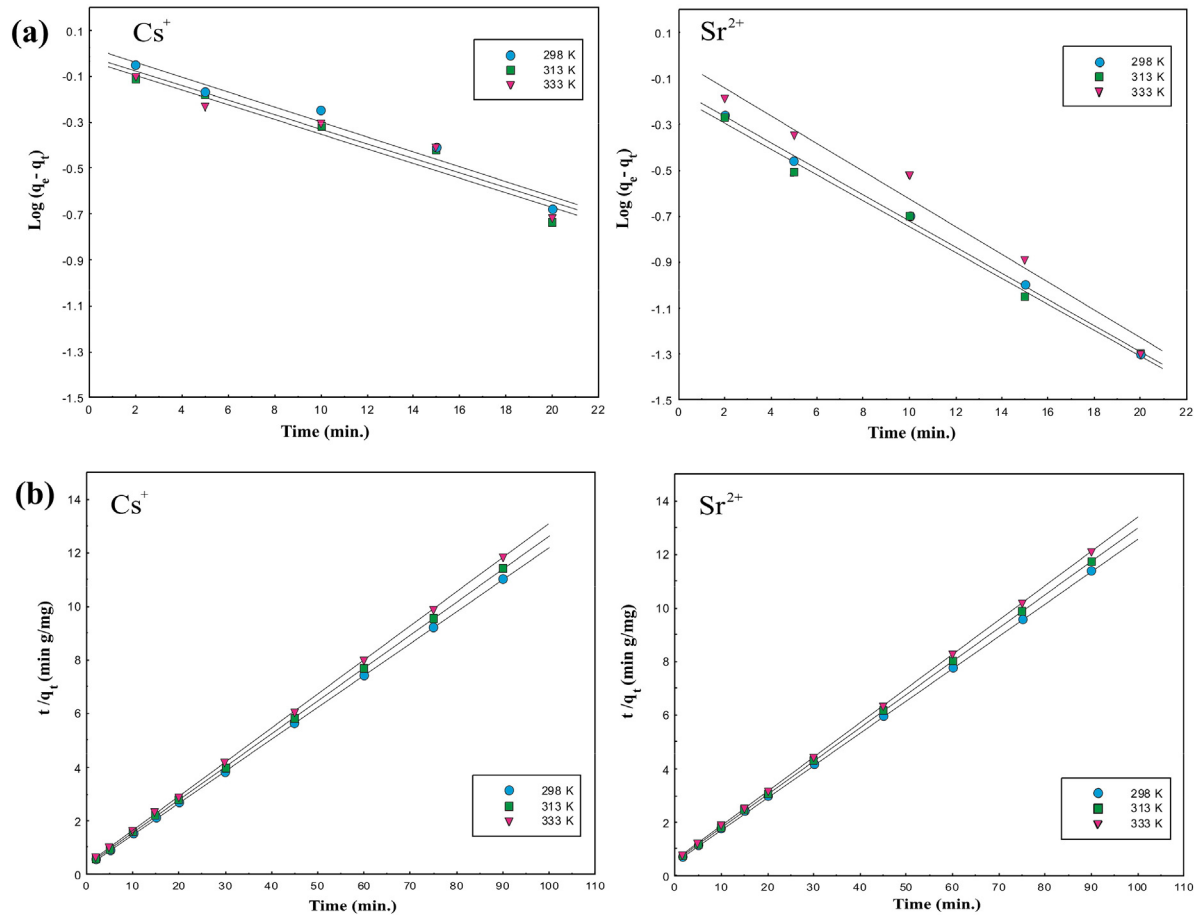


Fig. 5. Kinetic plots of Cs⁺ and Sr²⁺ ions onto the studied clay sample showing: a. Pseudo first second-order, b. Pseudo second-order.

the amount of adsorbate on the adsorbent and the concentration of dissolved adsorbate in the liquid at equilibrium (Mckay and Ho, 1999). In this concern, three widely used isotherms, Langmuir, Freundlich, and Dubinin-Radushkevitch (D-R) were tested with the obtained experimental data where the results reflect the efficiency of studied clay sample for the sorption of Cs⁺ and Sr²⁺ ions from aqueous solutions at different temperatures.

3.6.1. Langmuir isotherm model

The Langmuir sorption isotherm model is based on the monolayer coverage of sorption surfaces and assumes that sorption occurs on a structurally homogeneous sorbent and all the sorption sites are energetically identical. The Langmuir adsorption isotherm has been successfully applied to many other real adsorption processes as given by Langmuir (1918). The Langmuir isotherm applies to adsorption on completely homogenous surfaces with negligible interaction between adsorbed

molecules. This theory considers that all surface sites have the same adsorption energy. The Langmuir equation can be expressed as:

$$q_e = \frac{Q^0 b C_e}{1 + b C_e} \tag{13}$$

For fitting the experimental data, the Langmuir model was linearized as:

$$\frac{C_e}{q_e} = \frac{1}{Q^0 b} + \frac{1}{Q^0} C_e \tag{14}$$

where, q_e is the amount of metal ion sorbed per unit weight of clay (mg/g), C_e is the equilibrium concentration of the metal ion in the equilibrium solution (mg/l), Q^0 is the monolayer sorption capacity (mg/g) and b is the constant related to the free energy of adsorption ($b \propto e^{-\Delta G/RT}$).

Table 3 Results of the kinetic studies of Cs⁺ and Sr²⁺ sorbed onto studied clay.

Metal ion	Temp., (K)	First-order kinetic parameters			Second-order kinetic parameters				$q_{e, exp.}$ (mg/g)
		$k_1, (\text{min}^{-1})$	$q_{e, calc.}$ (mg/g)	R^2	$k_2, (\text{g/mg min})$	$q_{e, calc.}$ (mg/g)	h (mg/g min)	R^2	
Cs ⁺	298	0.076	1.067	0.960	0.312	8.403	22.030	0.999	8.35
	313	0.074	0.973	0.944	0.280	8.130	18.507	0.999	8.08
	333	0.071	0.928	0.931	0.270	7.813	16.482	0.999	7.79
Sr ²⁺	298	0.131	1.105	0.998	0.646	8.730	49.234	0.999	7.95
	313	0.129	0.951	0.999	0.604	8.692	45.633	0.999	7.70
	333	0.126	0.901	0.974	0.515	7.463	28.684	0.999	7.45

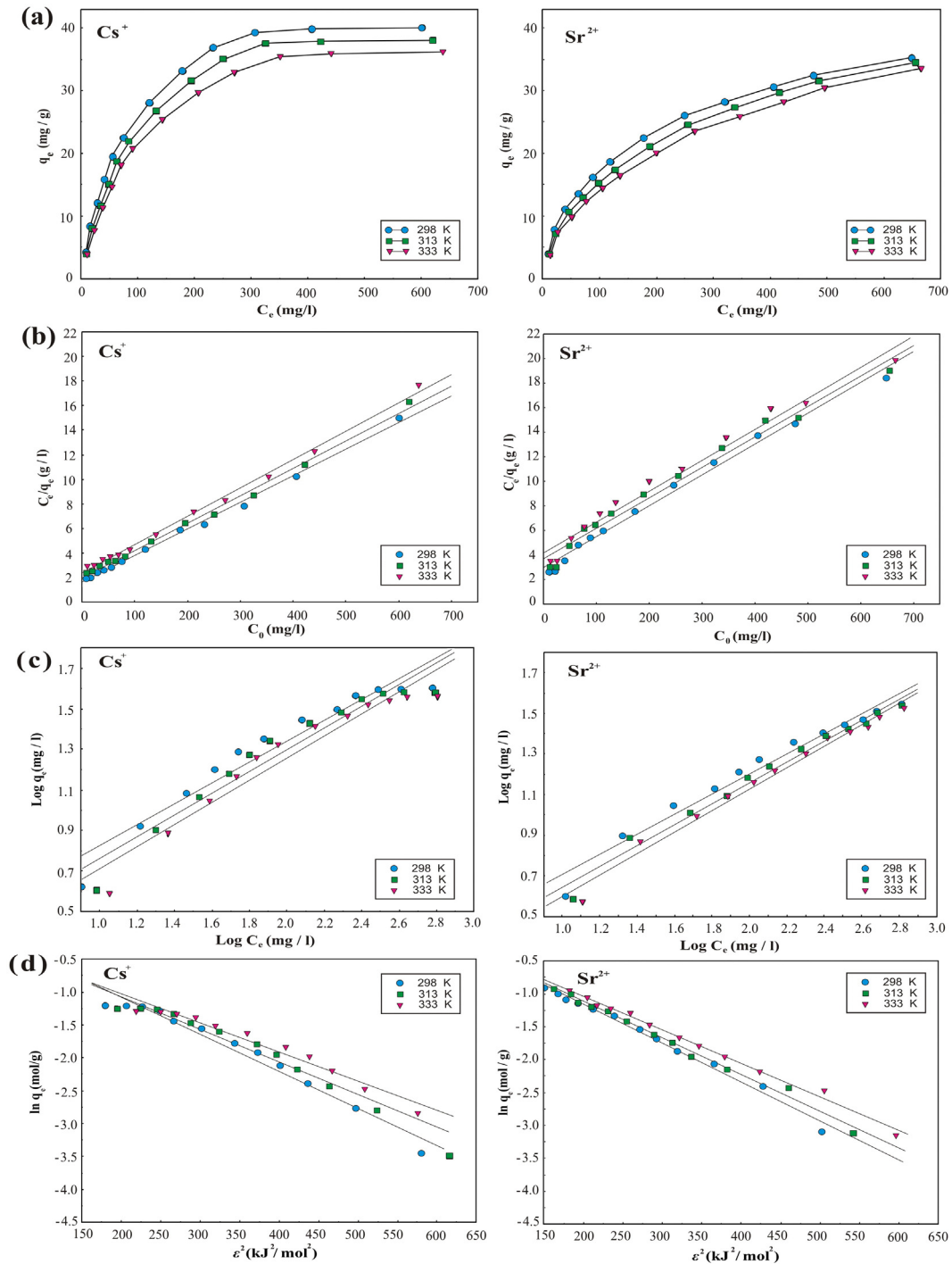


Fig. 6. Sorption of Cs + and Sr²⁺ ions onto the studied clay sample at different temperatures showing: a. Sorption isotherm, b. Langmuir Sorption isotherm analysis and c. D-R isotherm plots.

Table 4
Langmuir and Freundlich isotherm parameters for the sorption of Cs⁺, Sr²⁺ ions onto studied clay.

Metal ion	Temp., (K)	Langmuir model				Freundlich model		
		Q ⁰ , mg/g	b, l/mg	R ²	R _L	n	K _f , mg/g	R ²
Cs ⁺	298	46.296	0.013	0.997	0.071	1.946	2.051	0.935
	313	45.045	0.011	0.995	0.082	1.869	1.687	0.934
	333	43.478	0.010	0.996	0.092	1.835	1.469	0.931
Sr ²⁺	298	39.683	0.009	0.990	0.104	2.024	1.629	0.969
	313	39.526	0.007	0.980	0.129	1.942	1.340	0.982
	333	39.461	0.006	0.978	0.141	1.890	1.171	0.983

The Langmuir sorption isotherms of cesium and strontium ions onto studied materials are presented in Fig. 6b. The numerical values of Q⁰ and b for Cs⁺ and Sr²⁺ ions evaluated from the slope and intercept of C_e/q_e versus C_e are given in Table 4. The monolayer sorption capacity (Q⁰) values of Cs⁺ ions are relatively higher than that of Sr²⁺ ions for the studied clay. The Langmuir constants Q⁰ and b for the sorption of both ions decreased with temperature showing that the sorption capacity is enhanced by decreasing temperature. This decrease in sorption capacity at higher temperature may suggest that the active surface available for sorption has decreased with temperature. One of the essential characteristics of Langmuir isotherm model could be explained

in terms of a dimensionless constant separation factor R_L that can be expressed as:

$$R_L = \frac{1}{1 + bC_0} \quad (15)$$

where, C_0 is the highest initial metal ion concentration (mg/l).

The R_L value indicates the shape of the isotherm as follows: To be irreversible ($R_L = 0$), favorable ($0 < R_L < 1$), linear ($R_L = 1$) and unfavorable ($R_L > 1$) (Mohamed et al., 2016). The calculated value of R_L indicates that the sorption of Cs^+ and Sr^{2+} ions onto clay was favorable as shown in Table 4.

3.6.2. Freundlich isotherm model

The Freundlich sorption isotherm is one of the most widely used mathematical descriptions, usually fits the experimental data over a wide range of concentrations (Livia et al., 2015). The Freundlich model is represented by the equation:

$$q_e = K_f C_e^{1/n} \quad (16)$$

The Freundlich model is linearized as follows:

$$\log q_e = \log K_f + (1/n) \log C_e \quad (17)$$

where K_f is constant indicative of the relative sorption capacity of the sorbent (mg/g) and $1/n$ is the constant indicative of the intensity of sorption process.

The values of the constant n and K_f were calculated from the slope and the intercepts of the plot as in Table 4. The $1/n$ value is usually dependent on the nature and strength of sorption process as well as on the distribution of active sites. A feature indicating an increase tendency for sorption with increased the concentration (Fig. 6c). Also the K_f value for Cs^+ was greater than Sr^{2+} .

3.6.3. Dubinin-Radushkevich isotherm model

The Dubinin-Radushkevich (D-R) isotherm model describes sorption on a single type of uniform pores. The D-R model is represented by the equation:

$$\ln q_e = \ln q_m - \beta \varepsilon^2 \quad (18)$$

where q_m (meq g^{-1}) is the maximum adsorption capacity, β ($\text{mol}^2 \text{kJ}^{-2}$) is the constant related to the sorption energy and ε is Polanyi potential:

$$\varepsilon = RT \ln(1 + 1/C_e) \quad (19)$$

where, R is the gas constant ($\text{kJ/mol}\cdot\text{K}$) and T is the temperature (K).

The free energy change when one mole of ion is transferred from infinity in the solution to the surface of adsorbent is called as mean free energy change E (kJ/mol^{-1}):

$$E = (2\beta)^{-1/2} \quad (20)$$

The D-R plots of $\ln q_e$ versus ε^2 for the sorption of Cs^+ , Sr^{2+} ions at different temperatures resulted of q_m , β , E and the correlation factor (R^2) are given in The D-R plots for the sorption of both radionuclides at different temperatures are also given in Fig. 6d.

These D-R parameters are presented in Table 5. The magnitude of mean free energy of sorption (E) can be related to the reaction mechanism. If E is in the range of 8–16 kJ/mol, sorption is governed by ion exchange (Helfferich, 1962). In the case of $E < 8.0$ kJ/mol, physical forces may affect the sorption mechanism. The value of E for Cs^+ , Sr^{2+} ions were 9.167 and 10.040 kJ/mol; respectively, indicating that both cations are adsorbed through ion exchange process.

Table 5

D-R isotherm parameters for the sorption of Cs^+ , Sr^{2+} ions onto clay sample.

Metal ion	Temp., (K)	β , ($\text{mol}^2 \text{kJ}^{-2}$)	q_m , (mg/g)	R^2	E , (kJ/mol^{-1})
Cs^+	298	0.0057	1.058	0.969	9.382
	313	0.0054	1.042	0.968	9.587
	333	0.0050	1.025	0.965	10.040
Sr^{2+}	298	0.0060	1.032	0.989	9.167
	313	0.0056	1.028	0.992	9.475
	333	0.0051	1.023	0.993	9.901

3.7. Thermodynamic studies

Temperature is an extremely important parameter controlling the adsorption process. According to Priya et al. (2016), it can modify the equilibrium capacity of the adsorbent for a particular adsorbate. The values of the thermodynamic equilibrium constant (K_c) at three different temperatures were determined from the product of the Langmuir equation parameters Q^0 and b . Table 6 shows the variation of values K_c with temperature which decreased with increasing of temperature. The Gibbs free energy change, ΔG^0 , is the fundamental criterion of spontaneity, and given by the following equation:

$$\Delta G^0 = -RT \ln K_c \quad (21)$$

where, K_c is the sorption equilibrium constant, R is the gas constant ($\text{kJ/mol}\cdot\text{K}$) and T is the absolute temperature (K).

Reactions occur spontaneously at a given temperature if ΔG^0 is a negative quantity and non-spontaneous when the value is positive. There is another process to obtain the enthalpy change (ΔH^0) and entropy change (ΔS^0) by plotting of $\ln K_c$ versus $1/T$ (Fig. 7) which is proved as in Eq. (22). The free energy of the sorption reaction as Eq. (23):

$$\ln K_c = \frac{\Delta S}{R} - \frac{\Delta H}{RT} \quad (22)$$

$$\Delta G^0 = \Delta H^0 - T\Delta S^0 \quad (23)$$

The thermodynamic parameters (ΔH^0 , ΔG^0 and ΔS^0) for Cs^+ and Sr^{2+} ions sorbed by clay sample are given in Table 6. The change in ΔH^0 for Cs^+ and Sr^{2+} ions was found to be negative for the all adsorbents used, confirming the exothermic nature of the sorption processes in the studied clay sample. The reason of this behavior could originate from thermal destabilization which cause an increase in the mobility of Cs^+ and Sr^{2+} ions on the surface of the solid with increasing temperature, thus enhancing the desorption steps. The positive values of ΔG^0 indicate the non-spontaneous nature of Cs^+ and Sr^{2+} ions onto studied clay. Values of the ΔS^0 are negative for Cs^+ and Sr^{2+} ions as a result of a random reaction, since such reaction leads to transferring the sorbate ions from a disorder state in the solution to a more order state. This decrease in the disorder state in the solution to a more order state may be attributed to the probability of increase of mobility of Cs^+ and Sr^{2+} ions with dehydration steps as well as the surrounding water molecules within the body of solution. A feature suggests that the increasing of temperature from 298° to 333° K leads to slight decrease in the sorption of Cs^+ and Sr^{2+} ions.

Table 6

Values of thermodynamic parameters for sorption of Cs^+ and Sr^{2+} ions onto clay sample.

Metal ion	Temp., (K)	K_c	ΔG^0 , (kJ/mol)	ΔH^0 , (kJ/mol)	ΔS^0 , (J/mol·K)
Cs^+	298	0.610	1.226	−8.30	−32.93
	313	0.505	1.778		
	333	0.428	2.354		
Sr^{2+}	298	0.341	2.663	−8.11	−36.14
	313	0.272	3.391		
	333	0.241	3.940		

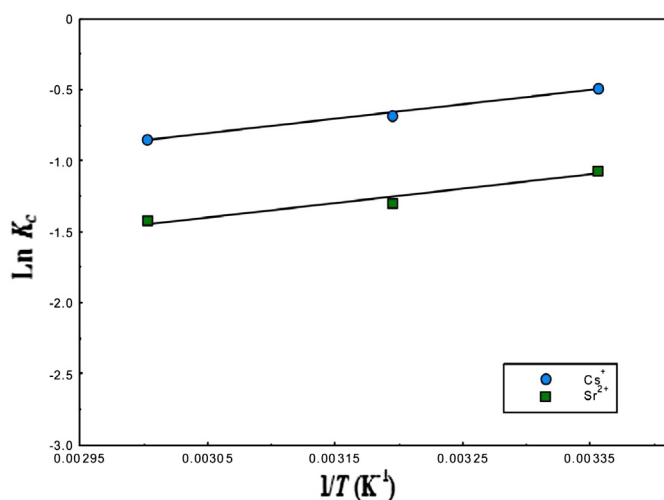


Fig. 7. Relationship between $\ln K_c$ and $1/T$ of sorption of Cs^+ and Sr^{2+} ions onto studied clay.

4. Conclusion

The level and the type of waste, the geochemistry of the clay and the role of climate, are important factors for controlling the geosphere medium of the studied area, as well as the selection of the site and method of burial of radioactive wastes. The kinetics of both metal ions was experimentally studied and the obtained rate data were analyzed using simple kinetic models. Results demonstrated that the pseudo second-order sorption mechanism is predominant and the over-all rate constant of each sorption process occurs to be controlled by chemical sorption process. The Cs^+ and Sr^{2+} ions sorption data were described using Freundlich, Langmuir and Dubinin–Radushkevich (D–R) models. The sorption in both of them ions increased with increasing initial metal ions concentration and the amount of Cs^+ ions sorbed onto clay is greater than that of Sr^{2+} ions, which it favored in the lower temperature of an aqueous solution. The maximum sorption capacity and the mean free energy of the studied ions have been determined. The sorption of each ion is an exothermic process. These results showed that natural materials an efficient ion exchange material for the behavior of cesium and strontium ions releasing on the surrounded geosphere of the disposal site.

Acknowledgement

The authors acknowledge the journal anonymous reviewers for their very constructive and helpful comments as well as for editorial comments and handling, which helped to improve the manuscript. The authors are grateful to the Hot Laboratories and Waste Management Center of Atomic Energy Authority of Egypt for the financial and academic support of this work.

References

- Abdel Moamen, O.A., Ismail, I.M., Abdel Monem, N., Abdel Rahman, R.O., 2015. Factorial design analysis for optimizing the removal of cesium and strontium ions on synthetic nano-sized zeolite. *J. Taiwan Inst. Chem. Eng.* 55, 133–144.
- Abdel Rahman, R.O., Zaki, A.A., 2011. Comparative study of leaching conceptual models: Cs leaching from different ILW cement based matrices. *Chem. Eng. J.* 173, 722–736.
- Abdel Rahman, R.O., Zaki, A.A., El-Kamash, A.M., 2007. Modeling the long-term leaching behavior of ^{137}Cs , ^{60}Co , and $^{152, 154}\text{Eu}$ radionuclides from cement–clay matrices. *J. Hazard. Mat.* 145, 372–380.
- Abdel Rahman, R.O., Ibrahim, H.A., Abdel Monem, N.M., 2009. Long-term performances of zeolite Na A-X blend as backfill material in near surface disposal vault. *Chem. Eng. J.* 149, 143–152.
- Alves, A.S.M., Frutuoso, M.P.F., Passos, E.M., Fontes, G.S., 2015. Stochastic and deterministic models to evaluate the critical distance of a near surface repository for the disposal of intermediate and low level radioactive wastes. *Nucl. Eng. Des.* 287, 57–67.
- Babechuk, M.G., Widdowson, M., Kamber, B.S., 2014. Quantifying chemical weathering intensity and trace element release from two contrasting basalt profiles, Deccan Traps, India. *Chem. Geo.* 363, 56–75.

- Bucur, C., Olteanu, M., Dulama, N., Pavelescu, M., 2011. Cesium sorption/desorption on salinized geologic formations. *Rom. J. Phys.* 56 (5–6), 769–783.
- Churchman, G.J., Gates, W.P., Theng, B.K.G., Yua, G., 2006. Clays and clay minerals for pollution control. In: Bergaya, F., Theng, B.K.G., Lagaly, G. (Eds.), *Handbook of Clay Science, Developments in Clay Science 1*. Elsevier Ltd., Netherlands, pp. 625–675.
- Darcy, D.L., Andrew, D.J., David, J.M., 2014. A reactive-transport model for examining tectonic and climatic controls on chemical weathering and atmospheric CO_2 consumption in granitic regolith. *Chem. Geol.* 365, 30–42.
- Deepthi Rani, R., Sasiidhar, P., 2011. Physico-chemical characterization of clays at Kalpakkam nuclear plant site towards assessment of radioactive waste disposal. *Nucl. Eng. Des.* 241, 2353–2358.
- Dupuis, C., Hebert, R., Cote, V.D., 2006. Geochemistry of sedimentary rocks melange and flysch units south of the Yarlung Zangbo suture zone, southern Tibet. *J. Asian Earth Sci.* 26, 489–508.
- Eduardo, G., Alberto, R., 2016. Provenance control on chemical indices of weathering (Taiwan river sands). *Sed. Geo.* 336, 81–95.
- Etemad, S.N., Hosseini, B.M., Armstrong, A.J.S., 2011. Petrography and geochemistry of clastic sedimentary rocks as evidences for provenance of the Lower Cambrian Lalun Formation, Posht-e-Badam block, Central Iran. *J. Afr. Earth Sci.* 61, 142–159.
- Frank, B., Karsten, S., Corina, D., Jin-Sheng, H., Thomas, S., Peter, K., 2014. Petrogenesis, permafrost, substrate and topography: plot and landscape scale interrelations of weathering processes on the central-eastern Tibetan Plateau. *Geoderma* 226 (227), 300–316.
- Harley, S.S.T., Angélica, F.D.C.V., Antônio, C.S.S., 2015. Technological properties of ceramic produced from steatite (soapstone) residues–kaolinite clay ceramic composites. *Appl. Clay Sci.* 112–113, 53–61.
- Helfferich, F., 1962. *Ion Exchange*. McGraw-Hill, New York.
- Hossain, I., Roy, K.K., Biswas, P.K., Alam, M.M., Deeba, F., 2014. Geochemical characteristics of Holocene sediments from Chuadanga district, Bangladesh: implications for weathering, climate, redox conditions, provenance and tectonic setting. *Chin. J. Geochem.* 33, 336–350.
- Kamel, N.H., Navratil, D.J., 2002. Migration of Cs in unsaturated soils at a site in Egypt. *J. Radioanal. Nucl. Chem.* 254 (3), 421–429.
- Langmuir, I., 1918. The adsorption of gases on plane surfaces of glass, mica and platinum. *J. Am. Chem. Soc.* 40, 1361–1403.
- Livia, M.P., Anne, H.F., Susanne, R., 2015. Sorption of norfloxacin in soils: analytical method, kinetic and thermodynamic isotherms. *Chemosphere* 119, 310–317.
- Martinez, R.E., Sharma, P., Kappler, A., 2010. Surface binding site analysis of Ca^{2+} -homoionized clay-humic acid complexes. *J. Colloid Interface Sci.* 352, 526–534.
- McKay, G., Ho, Y.S., 1999. Pseudo-second order model for sorption processes. *Process Biochem.* 34, 451–460.
- Mohamed, E.M., Gehan, M.N., Nabila, M.E., Heba, I.B., Sandeep, K., Tarek, M.A., 2016. Kinetics, isotherm, and thermodynamic studies of the adsorption of reactive red 195 A dye from water by modified Switchgrass Biochar adsorbent. *J. Indus. and Eng. Chem.* 37, 156–167.
- Ohta, T., Arai, H., 2007. Statistical empirical index of chemical weathering in igneous rocks: a new tool for evaluating the degree of weathering. *Chem. Geo.* 240, 280–297.
- Paola, B.A., Thiago, P.A.O., José, P., 2015. Identification of clay minerals in mixtures subjected to differential thermal and thermogravimetry analyses and methylene blue adsorption tests. *Appl. Clay Sci.* 114, 133–140.
- Po, N.C., Wang, M.K., Huang, P.M., Wang, J.J., Chiu, C.Y., 2010. Cesium and strontium sorption by selected tropical and subtropical soils around nuclear facilities. *J. Environ. Radio.* 101, 472–481.
- Priya, B., Pinaki, D., Aisha, Z., Papita, D., 2016. Application of graphene oxide nanoplatelets for adsorption of Ibuprofen from aqueous solutions: evaluation of process kinetics and thermodynamics. *Process Saf. Environ. Prot.* 101, 45–53.
- Runliang, Z., Lizhong, Z., Jianxi, Z., Xu, L., 2008. Structure of cetyltrimethylammonium intercalated hydrobiotite. *Appl. Clay Sci.* 42, 224–231.
- Roser, B.P., Korsch, R.J., 1988. Provenance signatures of sandstone-mudstone suites determined using discrimination function analysis of major element data. *Chem. Geol.* 67, 119–139.
- Sahraeyan, M., Bahrami, M., 2012. Geochemistry of sandstones from the Aghajari formation, folded Zagros Zone, southwestern Iran, implication for paleoweathering condition, provenance, and tectonic setting. *Inter. J. of Basic and Applied Sciences* 1 (4), 390–407.
- Sánchez-Jiménez, N., Gismera, M.J., Sevilla, M.T., Cuevas, J., Rodríguez-Rastrero, M., Procopio, J.R., 2012. Clayey materials as geologic barrier in urban landfills: comprehensive study of the interaction of selected quarry materials with heavy metals. *Appl. Clay Sci.* 56, 23–29.
- Schneider, S., Hornung, J., Hinderer, M., Garzanti, E., 2016. Petrography and geochemistry of modern river sediments in an equatorial environment (Rwenzori Mountains and Albertine rift, Uganda): implications for weathering and provenance. *Sediment. Geol.* 336, 106–119.
- Sener, C., 2015. New weathering indices for evaluating durability and weathering characterization of crystalline rock material: a case study from NE Turkey. *J. Afr. Earth Sci.* 103, 54–64.
- Seung, M.L., Diwakar, T., 2012. Organo and inorgano-organo-modified clays in the remediation of aqueous solutions: an overview. *Appl. Clay Sci.* 59, 84–102.
- Shaohao, Z., Chuanjun, W., Deru, X., Qiang, S., Xiaowen, Z., Pete, H., Maozhou, H., 2016. Provenance and depositional setting of Lower Silurian siliciclastic rocks on Hainan Island, South China: implications for a passive margin environment of South China in Gondwana. *J. Asian Earth Sci.* 123, 243–262.
- Sila, P., Cesar, V., Ian, C., Jesús, M.S., Fernando, G., Danielle, S., 2015. Climatic control on palaeohydrology and cyclical sediment distribution in the Plio-Quaternary deposits of the Guadix Basin (Betic Cordillera, Spain). *Quat. Intern.* 389, 56–69.
- Su, L., Richard, N., Gaschnig, M., Roberta Rudnick, L., 2016. Insights into chemical weathering of the upper continental crust from the geochemistry of ancient glacial diamictites. *Geochim. Cosm. Acta.* 176, 96–117.

- Suttner, L.J., Dutta, P.K., 1986. Alluvial sandstone composition and paleoclimate framework mineralogy. *J. Sediment. Petrol.* 56, 329–345.
- Talal, S., 2014. Sorption kinetics: obtaining a pseudo-second order rate equation based on a mass balance approach. *J. Envy. Chem. Eng.* 2, 1001–1006.
- Tianlik, T., Nik, N.N., Mohammad, S., Yoonsing, W., Abdul-Kadir, M., 2016. Risk assessment of metal contamination in soil and groundwater in Asia: a review of recent trends as well as existing environmental laws and regulations. *Pedosphere* 26 (4), 431–450.
- Van der Marel, H.W., Beutelspacher, H., 1976. *Atlas of Infrared Spectroscopy of Clay Minerals and Their Admixtures*. Elsevier Scientific Pub. Co., Amsterdam.
- Voicu, G., Bardoux, M., 2002. Geochemical behavior under tropical weathering of the Barama-Mazaruni greenstone belt at Omai gold mine, Guiana Shield. *Appl. Geochem.* 17, 321–336.
- Voicu, G., Bardoux, M., Harnois, L., Grepeau, R., 1997. Lithological and geochemical environment of igneous and sedimentary rocks at Omai gold mine, Guyana, South America. *Explor. Min. Geol.* 6, 153–170.
- Zaki, A.A., 2000. Performance Assessment of Radioactive Waste Disposal Facility Ph.D. Thesis University of Alexandria, Egypt (222 pp).
- Zaki, A.A., Ahmad, M.I., Abdel Rahman, R.O., 2011. Evaluation of the use of natural clay as a barrier for the retardation of some radionuclides. *Special Issue on Radioactive Waste Management Science and Technology for IJES* 2, 239–254.
- Ziemer, S.P., Niederhauser, T.L., Woolley, E.M., 2006. Thermodynamics of complexation of aqueous 18-crown-6 with rubidium and cesium ions: apparent molar volumes and apparent molar heat capacities of aqueous (18-crown-6 + rubidium chloride) and (18-crown-6 + cesium chloride) at temperatures (278.15 to 393.15) K, at molalities (0.02 to 0.33) mol. kg⁻¹, and at the pressure 0.35 MPa. *J. Chem. Thermodynamics* 38, 323–336.